Mott-Hubbard type insulating nature of epitaxial $LaVO_3$ thin films

Anupam Jana, R. J. Choudhary,* and D. M. Phase
UGC-DAE Consortium for Scientific Research, Indore 452001, Madhya Pradesh, India

(Received 22 January 2018; revised manuscript received 29 May 2018; published 13 August 2018)

The electronic structure of epitaxial $LaVO_3$ (00l) thin films have been studied using resonant photoemission spectroscopy (RPES) and x-ray absorption near edge spectroscopy (XANES) measurements. The RPES study confirms the mixing of V 3*d* with O 2*p* states and the V 3*d* character at 6.9 eV and 1.5 eV binding energies, respectively. The resonant behavior of V 3*d* state suggests $3d^{n-1}$ final state, ascribed with an incoherent structure, and is attributed as a lower Hubbard band. The smaller value of crystal field splitting energy observed in O *K*-edge XANES spectrum and the hopping parameter obtained from simulations reveal a weaker hybridization between ligand O 2*p* and metal V 3*d* orbitals. Combined spectra of occupied and unoccupied states suggest the Mott-Hubbard type insulating nature of the epitaxial $LaVO_3$ thin films at room temperature, different from its bulk counterpart, which is placed intermediate between the charge transfer and Mott-Hubbard regime.

DOI: 10.1103/PhysRevB.98.075124

I. INTRODUCTION

Transition metal (TM) oxides manifest a wide spectrum of fascinating properties such as metal-insulator transition, superconductivity, and colossal magnetoresistance [1,2], and consequently have attracted tremendous attention among the condensed matter physicists over the last few decades. These properties emanate due to competing energetics such as Coulomb correlations, bandwidth, charge transfer gap, etc., which shape up their unique electronic structure. Among these materials, perovskite $LaVO_3$ (LVO) represents an interesting system that shows a strong spin, charge, and orbital coupled phenomena, which lead to exotic electronic, magnetic, and electrical properties [3–6]. Single-crystal Mott insulator LVO exhibits spin ordering (SO) and orbital ordering (OO) within a narrow temperature window making it an interesting system to probe the electronic correlation effects. LVO has a $GdFeO_3$-type orthorhombic structure with lattice parameters $a = 5.55548$ Å, $b = 7.84868$ Å, and $c = 5.55349$ Å at room temperature [7]. LVO goes through an orthorhombic to monoclinic structure along with *G*-type OO state by first-order phase transition below 141 K due to distortion in VO_6 octahedra. It also undergoes a magnetic transition from a paramagnetic to an antiferromagnetic state along with the *C*-type SO state below 143 K [8]. Interestingly, a few reports reveal anomalous diamagnetic behavior of LVO, which vanishes upon application of external high pressure [5,9]. The origin of these properties is intimately related to the structural property as well as the precise details of their electronic structure.

The electronic properties of LVO have been studied in the past and the nature of the gap opening at the Fermi level has been debated and compared with other orthovanadates [10–14]. The valence-band spectra of such materials are known to reveal coherent and incoherent features. The dynamical mean-field theory (DMFT) ascribed quasiparticle excitations to the coherent structure, whereas the incoherent structure was assigned to the lower-Hubbard band [15,16]. It has been shown that the coherent feature disappears by the Mott-Hubbard screening in $LaVO_3$, similar to YVO_3 and opens an insulating gap [11]. Divalent Ca or Sr substitution in $LaVO_3$, besides doping holes in the system, changes the bandwidth (W) by changing the V-O-V bond angle, yielding a modification in the electronic structure *vis a vis* electrical and magnetic properties [4,17–20]. It is argued that the alteration in VO_6 octahedra upon external pressure or chemical pressure is one of the important factors for the observed modifications in the various physical properties.

Besides the enormous importance of $LaVO_3$ as a Mott insulator for understanding the fundamental physics aspects of electron correlation effects, it possesses several technological applications also such as resistive random-access memory devices [21], and as an absorbing material in solar cells [22,23]. These applications hugely rely on the modifications in the electronic structure of LVO in thin film form. In recent years, thin films of LVO have also been explored for probing multifunctional behavior in various heterostructure systems arising due to charge transfer across the interface of such a heterostructure [24]. The epitaxially grown films have an important epitaxial strain effect, which causes changes in unit cell parameters, akin to an external/chemical pressure. These changes will have consequences upon various physical properties of such heterostructures via modifications in the electronic structure. Although there are reports available in literature on the electronic properties of $LaVO_3$ or related systems in their bulk form, such investigations are *rather limited* when it comes to the thin film form [25–27]. Wadati *et al.* studied the electronic structure of $LaVO_3/LaAlO_3$ multilayers by means of hard x-ray photoemission spectroscopy and found that the valence of V was partially converted from 3+ to 4+ at the interface on the side of the LVO layer. They attributed it to electronic reconstruction to eliminate the polar catastrophe at the interface [25]. Similar reports on thin films of $LaVO_3$ based systems also investigated the evolution and distribution

*Corresponding author: ram@csr.res.in

of V^{4+}/V^{3+} states at the surface and across the thickness of the films, as probed by x-ray photoelectron spectroscopy [26,27]. However, a comprehensive knowledge of the electronic structure comprising of the occupied and unoccupied states is lacking. In the present study, we have investigated the detailed electronic structure of epitaxial $LaVO_3$ thin film by probing the occupied and unoccupied states of $LaVO_3$ by performing resonant photoemission spectroscopy (RPES) and x-ray absorption near edge spectroscopy (XANES) measurements. It is observed that the epitaxial $LaVO_3$ film displays the Mott-Hubbard type insulating nature rather than it being intermediate between the charge transfer and Mott-Hubbard regime as reported earlier in the case of its bulk counterpart [11,12,28].

II. EXPERIMENTAL

An LVO thin film of thickness 40 nm was deposited on the (001) oriented $LaAlO_3$ (LAO) single-crystal substrates by pulsed laser deposition (PLD). The PLD system consists of a KrF excimer laser (Lambda Physik,) with a 20-ns pulse width and wavelength of 248 nm, external optics, and a vacuum chamber. To grow the LVO thin film, a dense pellet of $LaVO_4$ was used as a target for deposition. $LaVO_4$ was synthesized using a conventional solid-state reaction route. For the preparation of $LaVO_4$, stoichiometric amounts of La_2O_3 and V_2O_5 were mixed and annealed at 600 °C for 6 hours in air, followed by a second annealing at 1100 °C for 20 h, with an intermediate grinding for 12 hours. Finally, the $LaVO_4$ target was sintered at 1150 °C for 12 h. Deposition was carried out with a laser beam focused at the $LaVO_4$ single-phase polycrystalline target with a repetition rate of 3 Hz and a fluence of $\approx 1.8\,J/cm^2$. During deposition, the temperature of the substrate was kept at 600 °C under a vacuum near $\approx 2\times10^{-6}$ Torr. After deposition, the LVO thin-film sample was cooled to the room temperature at the rate of 10 °C/ min in the same pressure as used during deposition. The distance between the target and substrate was maintained at 4.5 cm during deposition. The thickness of the film was measured using stylus profilometer.

The crystalline phase was identified by a Bruker D2 Phaser x-ray diffractometer using Cu K_α ($\lambda = 1.5406$ Å) radiation. The in-plane phi scan was done by a Bruker D8-Discover high-resolution x-ray diffractometer. The x-ray photoemission spectroscopy (XPS) measurements were carried out using the Omicron energy analyzer (EA-125, Germany) with Al K_α (1486.6 eV) x-ray source. Valence-band (VB) measurements were performed at different photon energy values in the range of 30–68 eV at the angle integrated photo emission spectroscopy (AIPES) beamline on Indus-1 synchrotron source at RRCAT, Indore, India. The vacuum in the experimental chamber during measurements was of the order of 10^{-10} Torr. Prior to the photoemission measurements, the surface of the LVO thin film was cleaned using 500-eV Ar^+ ions. For determination of the Fermi level (E_F), the Au foil was kept in an electrical contact with the sample on the same sample holder and the Fermi level was aligned using the valence-band spectrum of the foil. The background of the core-level and the VB spectra was corrected using the Shirley method. The experimental resolution was estimated to be 0.30 eV in the studied range of photon energy used to record the VB spectra. To investigate the unoccupied states of the LVO film, x-ray absorption near edge spectroscopy across the V $L_{3,2}$ and O K edges was carried out at the room temperature in the total electron yield (TEY) mode at the beam line BL-01, Indus-2 at RRCAT, Indore, India. The energy resolution during XANES measurements across the measured energy range was estimated to be ~250 meV.

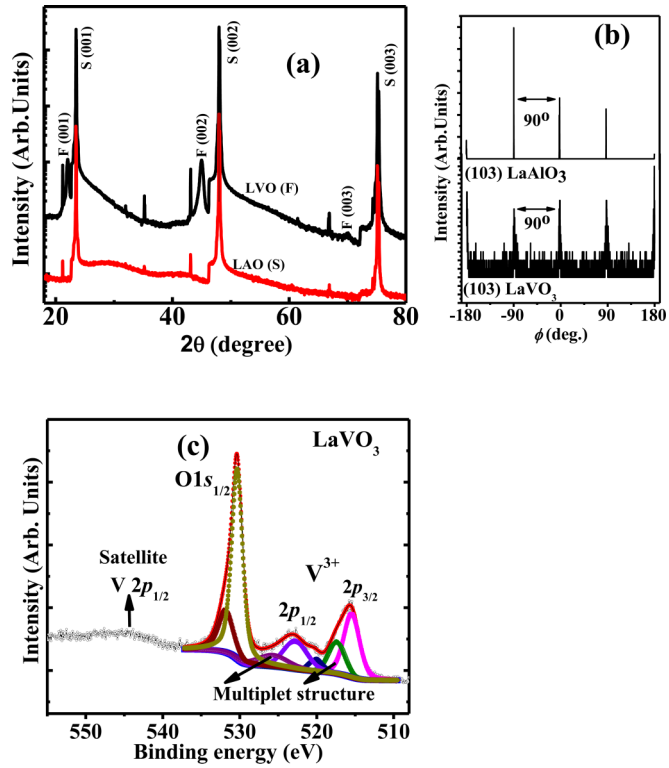

FIG. 1. (a) θ–2θ XRD pattern and (b) in-plane ϕ scans recorded along the (103) direction of the $LaAlO_3$ substrate and $LaVO_3$ film. (c) Deconvoluted V $2p$ and O $1s$ core level x-ray photoemission spectrum of $LaVO_3$ thin film.

III. RESULTS AND DISCUSSION

A. Crystal structure

Figure 1(a) shows the $\theta - 2\theta$ x-ray diffraction (XRD) patterns of the LVO thin film grown on the (00l) oriented LAO substrate. The diffraction pattern indicates that the growth of the film is in a single phase with the pseudocubic structure oriented along the [00l] direction. The influence of the LAO substrate on the grown film can be deduced from the lattice parameter of the deposited LVO film. The pseudocubic out-of-plane lattice parameter was calculated to be equal to 4.012 ± 0.003 Å. It should be noted here that the lattice parameter of the bulk pseudocubic $LaVO_3$ is 3.93 Å, which is larger than the cubic LAO (3.792 Å) substrate. Thus the resultant lattice mismatch $[(a_{\text{bulk-LVO}} - a_{\text{substrate}})\times100\%/a_{\text{substrate}}]$ between the bulk and the substrate of 3.5% will give rise to in-plane compressive strain and consequently, the out-of-plane lattice of LVO becomes slightly elongated. The resulting strain in the out-of-plane direction is found to be 2.1% using the

formula strain $\% = (c_{\text{film}} - c_{\text{bulk}}) \times 100\%/c_{\text{bulk}}$. Figure 1(b) depicts the azimuthal in-plane Φ scans for the film and the substrate along the (103) reflection. The Φ scans of the LVO thin film and LAO substrate show four diffraction peaks separated by 90°, which indicate the fourfold symmetry of the structure. Moreover, the peak positions in the Φ scans of the substrate and those of the films match together, suggesting the cube-on-cube epitaxial growth of $LaVO_3$ on the LAO substrate with the relations [001]F‖ [001]S and [100]F‖ [100]S.

B. Electronic properties

1. Chemical valence state

In order to investigate the chemical valence state, the core-level spectra of vanadium and oxygen have been studied by XPS. Figure 1(c) shows the V $2p$ and O $1s$ core-level photoemission spectra of the LVO thin film. We have fitted the core-level spectrum with a combination of the Gaussian and Lorentzian functions to estimate the position of individual features. The background of the spectrum is corrected by the Shirley method. The binding energy (E_B) positions deduced from the deconvolution of V $2p_{3/2}$ and V $2p_{1/2}$ are 515.6 and 522.8 eV, split by 7.2 eV due to the spin-orbit interaction, in conformity with the V^{3+} state in $LaVO_3$ bulk [29]. Asymmetry and broadening in the V $2p$ photoelectron spectrum arise due to the occurrence of multiplet structure owing to the presence of unpaired electrons in the V^{3+} state [30,31]. The V $2p_{1/2}$ feature is more broadened than the V $2p_{3/2}$ feature due to the Coster-Kroning effect [32]. The O $1s$ feature appears at 530.3 eV, which represents the lattice oxygen. The peak around 520 eV is due to an x-ray satellite of Al $K_{\alpha 3}$ source [33]. A feeble intense broad feature appearing at 544 eV is due to the satellite structure of V $2p_{1/2}$ state [11]. The cluster model suggests that the main peaks of V $2p_{3/2}$ and V $2p_{1/2}$ states correspond to the well-screened $\underline{c}3d^3\underline{L}$ ($\underline{c}$: hole in core level, $\underline{L}$: hole in O $2p$ band) final state configuration, whereas the charge transfer satellite structure corresponds to a poorly screened $\underline{c}3d^2$ configuration appearing at higher binding energy side of O $1s$ peak [11]. The asymmetry observed in the higher binding energy side of O $1s$ spectrum is due to the satellite structure of V $2p_{3/2}$. The position of satellite structure corresponding to the V $2p_{3/2}$ state ($E_B = 531.8$ eV) is hidden within the O $1s$ core level ($E_B = 530.3$ eV) and mixed with the states due to sample surface impurities [26,34] and hence its intensity is rather high. Here we preclude the possibility of oxygen deficient state at the higher binding energy of O $1s$ line because the oxygen vacancy should cause the appearance of V^{2+} state around 514 eV, which is absent.

2. Valence-band spectra

The valence-band spectrum (VBS) of the epitaxial $LaVO_3$ thin film recorded at photon energy of 52 eV at room temperature is shown in Fig. 2(a). Absence of spectral intensity at the Fermi energy (E_F) is confirming the insulating nature of the LVO film, shown in the inset of Fig. 2(a). In previous reports [11,19], it has been shown that spectrum in the energy range between $E_B = 0.5$ to 3.0 eV is due to the vanadium $3d$ character and the energy region between 3 to 9 eV is dominated by the O $2p$ contribution. The observed VB spectrum was fit

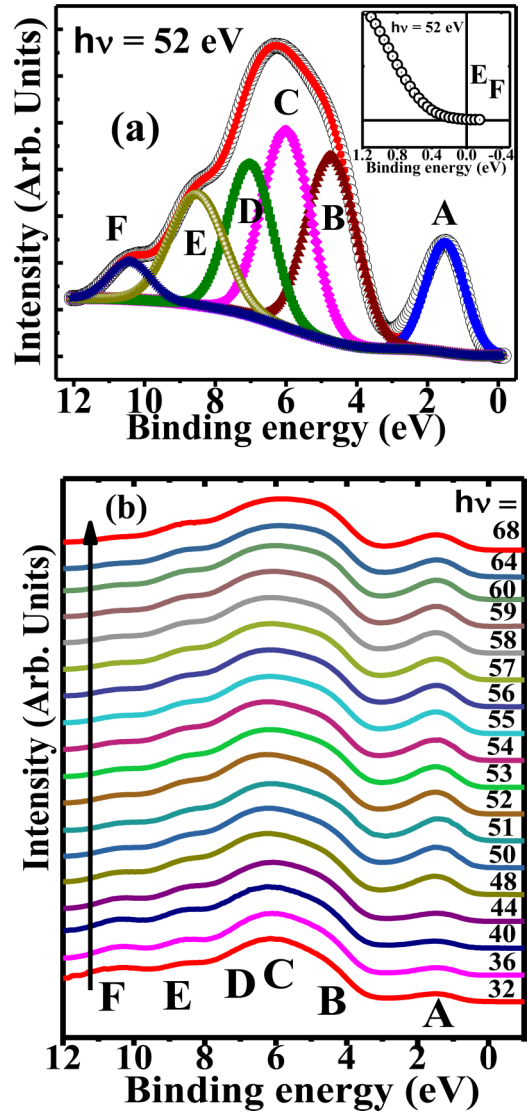

FIG. 2. (a) Room-temperature deconvoluted valence-band photoemission spectrum of $LaVO_3$ thin film recorded at 52 eV photon energy. (Inset) Zoomed view near E_F; absence of spectral intensity confirming the insulating nature of $LaVO_3$ thin film. (b) Energy distribution curves for the photon energies between 32 to 68 eV.

with the smallest number of the Gaussian functions that could adequately reproduce the major features of the spectrum. The vanadium $3d$ band is fitted with the Gaussian peak centered at $E_B = 1.5$ eV marked as A, and this feature is about 2.1 eV wide. Broadness of the V $3d$ band was discussed by Egdell *et al.* [35] in their photoemission spectroscopy study on bulk $LaVO_3$ in terms of strong electron-phonon interaction, related to the strong polarization of the lattice by a valence electron. This feature was termed as an incoherent structure of the insulating $LaVO_3$ material [11,19]. The O $2p$ band is fitted with the four Gaussian peaks marked as B, C, D, and E centered at 4.7, 5.9, 6.9, and 8.4 eV, respectively. The feature B arises owing to the nonbonding character of O $2p$ state and feature D is attributed to the bonding bands arising from the O $2p$ and V $3d$ hybridization [19]. The origin of feature C around 5.9 eV could be related to the Mott-Hubbard screened $3d^2\underline{D}$

(D denotes a hole in the nearest-neighbor V 3*d* state) configuration as suggested by R. J. O. Mossanek *et al.* [12], whereas feature E is attributed to the La 6*p* and O 2*p* hybridized states. A weak feature is observed at around 10.3 eV assigned as "F." A similar structure was observed around 10 eV by Smith and Henrich, in the angle integrated UPS spectra of cleaved V_2O_3, and was assigned to a satellite structure of vanadium [36].

(a) Resonant photoemission spectroscopy. To further understand the VBS, we performed RPES measurements. For the RPES study, the valence-band spectra of the epitaxial $LaVO_3$ film were recorded at room temperature (300 K), for different photon energy values swept through V $3p \rightarrow 3d$ excitation. Figure 2(b) depicts the energy distribution curves (EDCs) of the epitaxial LVO film for photon energy varying from 32 to 68 eV. From the EDCs, it is clearly observed that the intensity of the feature A at $B_E = 1.5$ eV increases with the photon energy, and it reaches maximum at about 52 eV and finally decreases with the increase in the photon energy. The calculated atomic O 2*p* photoionization cross section [37] suggests that the spectral weight of the O 2*p* band should decrease gradually with the photon energy. Therefore the observed photoemission enhancement is ascribed to the resonant photoemission intensity of the V 3*d* derived states. A small photoemission enhancement is also seen for the O 2*p* band (3 to 9 eV in VBS) within the given photon energy range, which is suggestive of mixed O 2*p* and V 3*d* character in this band as discussed later in the manuscript.

The photon energy dependence of the spectral intensity is revealed more clearly in the constant initial state (CIS) spectra. The CIS spectra are plotted by taking the area under the partial feature for all photon energy values. It is important to mention that removal and addition of an electron from a nonbonding orbital does not change the energy of the molecule; thus the RPES and CIS spectra were normalized to the intensity of O *2p* nonbonding state. The CIS of feature A shows a strong resonant enhancement with the maximum around 52 eV as shown in Fig. 3(a). The observed resonance profile is quite broad and extended over a large energy range. This behavior is quite different from the late transition-metal oxides, which show much narrower Fano-like resonance profiles [38], though, the broad nature of resonance behavior is quite common in the light transition-metal oxides [39–42]. The reason for the large width in the resonance profile was explained in terms of the shakeup excitation that essentially acts as a loss accompanying the $3p \rightarrow 3d$ optical absorption as mentioned by Barthe *et al.* [41].

The origin of the resonance around 52 eV photon energy can be explained on the basis of the quantum-mechanical interference between two excitation processes, which transform a certain initial state to the same final state via two possible channels. One of the photoemission channels is due to the direct photoemission from 3*d* state:

$$\mathrm{V}:\ 3p^6 3d^2\left(t_{2g}^2\right) + h\upsilon \rightarrow\ \mathrm{V}:\ 3p^6 3d^1\left(t_{2g}^1\right) + e^-.$$

The other channel of photoemission is due to the intraatomic excitation process at the resonant photon energy 52 eV by the 3*p* state followed by super Coster-Kronig decay. It is represented as

$$\mathrm{V}:\ 3p^6 3d^2 + h\upsilon \rightarrow\ [3p^5 3d^3]^* \rightarrow\ \mathrm{V}:\ 3p^6 3d^1 + e^-.$$

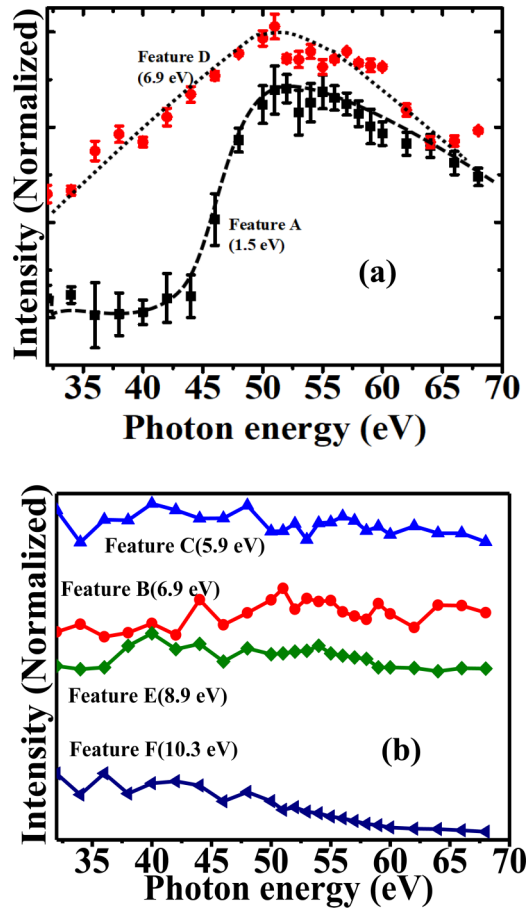

FIG. 3. (a) Constant initial state (CIS) spectra of feature A ($E_B = 1.5$ eV) and feature D ($E_B = 6.9$ eV) in the valence band of the $LaVO_3$ thin film, error bars represent the standard deviation of data. The lines in these spectra are guide to the eye. (b) Constant initial state (CIS) spectra of features "B," "C," "E," and "F" in the valence band of the $LaVO_3$ thin film.

The final state is indistinguishable in the two cases and consequently, the V 3*d* photoelectron yield increases dramatically and exhibits resonance. The resonance profile of feature A demonstrates its V-3*d* character. A similar resonant photoemission at around 52 eV was also observed in the isoelectronic V_2O_3 [40,43].

It should be noted here that the gap between 3*p* and 3*d* states is around 40.5 eV for V^{3+}, so one may expect the resonance of the V-3*d* photoemission to occur around this value of photon energy. However, the photon energy dependence profile exhibits a delay in the onset of the 3*p* to 3*d* resonance than the ground state 3*p* to 3*d* energy level separation in $LaVO_3$. These delays have been explained in terms of exchange interaction between the 3*p* hole and $n + 1$ 3*d* electrons [42]. Due to the extended nature of the 3*d* wave function, it overlaps with the 3*p* wave function significantly in the case of lighter transition metal elements where the 3*d* wave function is collapsed. As a result, the exchange interaction is so large that it causes the resonance peak far above the threshold by raising the optically favored $3p^5 3d^3$ multiplets [40].

Owing to the local nature of the resonant photoemission process, it has been used as a tool to distinguish the TM

d-like state contribution to the complex hybridized state in valence band [38]. Figure 3(a) also shows the photon energy dependence of the CIS intensity for feature D in the O $2p$ dominant region of VB. It is well known that the O $2p$ cross section gradually decreases with photon energies, however, we observed a resonance enhancement of feature D (E_B = 6.9 eV) as the photon energy is swept through the V $3p \rightarrow 3d$ excitation. The CIS intensity of feature D attains a maximum at 52 eV of the photon energy. The resonant enhancement of feature D also at 52 eV suggests that at binding energy 6.9 eV, an appreciable amount of V $3d$ character is present. Usually, resonance in the ligand emission, upon sweeping the photon energy through the metal $3p$ to $3d$ transition, is attributed to the metal d state hybridization with the ligand states [38,43]. Such resonant enhancement in O $2p$ band was also observed in YVO_3 and $CaVO_3$ [44] and was attributed to O $2p$ and V $3d$ hybridization. In other vanadium oxides too, like V_2O_3, V_2O_5, and VO_2, some O $2p$ bands show a resonance effect, which was also explained in terms of the hybridization between O $2p$ and V $3d$ orbitals [43]. Interestingly, Smith and Henrich [39] noticed a stronger resonance in the O $2p$ emission from Ti_2O_3 as compared to the O $2p$ emission from V_2O_3, despite an increased d character in the O $2p$ band in V_2O_3. However, Shin *et al.* [43] observed that the resonance effect of the V $3d$ band in VO_2 was weaker than the Ti $3d$ band in Ti_2O_3, even though both compounds had the same $3d^1$ electron configuration. It was also observed that in case of V_2O_5 with $3d^0$ electrons, the resonance effect of O $2p$ band was much stronger than that in VO_2 with $3d^1$ electrons. Therefore, based on the number of $3d$ electrons, the analysis of observed resonance enhancement in O $2p$ bands in RPES requires precaution for a quantitative discussion [43]. The CIS spectra of other features like B (E_B = 4.7 eV), C (E_B = 5.9 eV), E (E_B = 8.4 eV), and F (E_B = 10.4 eV) do not reveal any such resonance enhancement, as shown in Fig. 3(b), pointing out towards their O $2p$ character.

(b) X-ray absorption near edge spectroscopy. Figure 4(a) shows the V $L_{3,2}$ and O K-edge absorption spectrum of the strained $LaVO_3$ thin film along with the isoelectronic V_2O_3 and V_2O_5 samples measured at room temperature. In the case of vanadates, the relative positions of the vanadium L edge and oxygen K edge are such that these spectra are taken together. The position and intensity ratio of L_3: L_2 absorption peaks of strained $LaVO_3$ film resemble those of V_2O_3 confirming the V^{3+} valence state in the $LaVO_3$ thin film. The absence of any other phase with V^{5+} state (like $LaVO_4$) in the studied LVO film is ensured by comparing its XANES spectrum with that of the V_2O_5. The vanadium $L_{3,2}$ absorption spectrum corresponds to the transition from the V $2p$ core level to the unoccupied V $3d$ states. In the $LaVO_3$ film, two broad peaks centered at the position of around 517.8 and 524.2 eV are assigned to L_3 (V $2p_{3/2}$–V $3d$) and L_2 (V $2p_{1/2}$–V $3d$) transitions, respectively, owing to the spin-orbit coupling. These spectra agree well with the previous x-ray absorption spectrum (XAS) measurements of the single-crystal $LaVO_3$ [45] and other RVO_3 compounds [46,47]. The overall shape of the spin-orbit split V $L_{3,2}$ absorption is determined by the crystal field (CF) effects along with the multiplet effects, which are originated by $3d$-$3d$ Coulomb interaction and the $2p$-$3d$ Coulomb and exchange interactions [48]. Apart from the CF

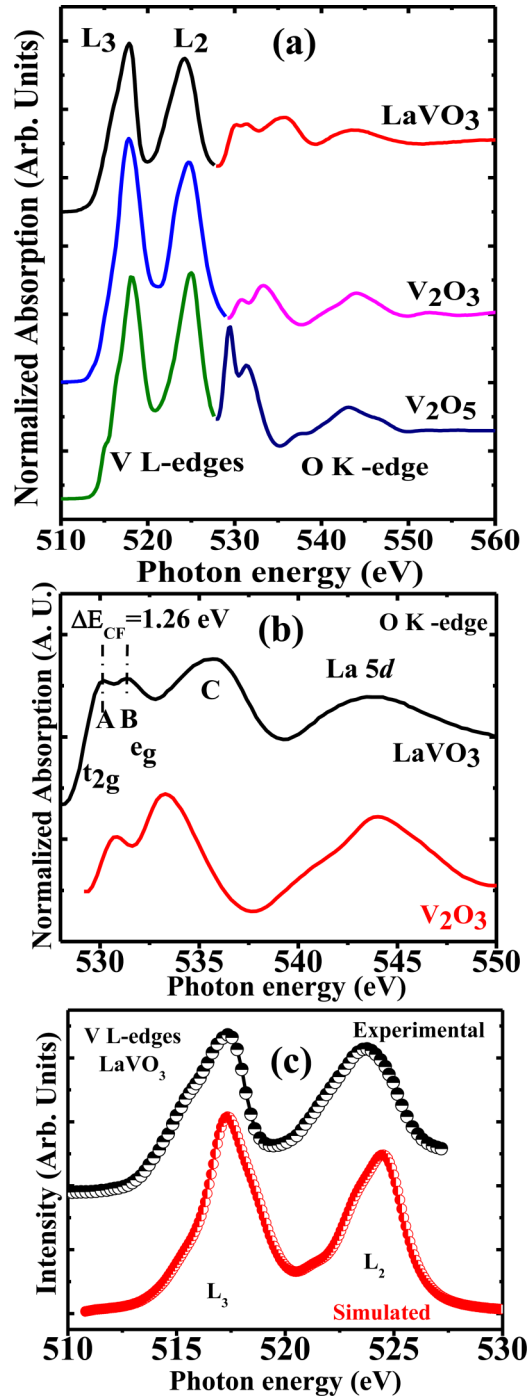

FIG. 4. (a) Room-temperature x-ray absorption near edge spectrum (XANES) of the $LaVO_3$ thin film along with V_2O_3, and V_2O_5 as references; (b) O K-edge x-ray absorption near edge spectrum of the $LaVO_3$ thin film along with isoelectronic V_2O_3. (c) Simulated V^{3+} L-edge spectra along with the experimental V L edge of the $LaVO_3$ thin film.

and multiplet states, the core-hole lifetime also contributes to the broadening of V $L_{3,2}$ absorption peaks [49]. The V L_2 peak is more broadened than the L_3 peak due to the Coster-Kroning Auger decay process into the $2p_{3/2}$ core hole [48]. The V $2p$ spin-orbit splitting derived from the V L_3 and V L_2 peaks is about 6.4 eV. However, a 7.2 eV splitting is observed in the

V $2p$ core level x-ray photoemission spectrum. The observed 0.8 eV disparity in spin-orbit splitting energy obtained from the XPS and XAS measurements arises because of the different final states of the excited electrons attained in the XAS and XPS processes. The final state of the excited electrons in XAS is $2p^5 3d^{n+1}$, which is $2p^5 3d^n$ in XPS considering $2p^6 3d^n$ as a ground state. Thus the Coulomb and exchange interaction between the ground and final states would be different in the two processes. As a result, one observes a disparity in spin-orbit splitted energy of $2p$ state from XAS and XPS measurements [49,50]. The pre-peak structure below the V L-edge spectrum, mostly assigned to multiplet splitting, is found to be less evident in the present case of strained LVO thin film compared to that in bulk and single crystal [45]. It has been shown that the appearance of the pre-edge feature in V L-edge spectrum depends on several parameters like Slater integral, V $3d$-O $2p$ hybridization, and crystal field strength [48,51]. We shall elaborate more over this in detail later in the manuscript.

The O $1s$ absorption spectrum starts from 528 eV corresponding to the transitions from the O $1s$ core level to the O $2p$ states hybridized with the V $3d$ states [separately shown in Fig. 4(b)]. Two distinct features marked as A and B at positions 530.1 and 531.4 eV arise due to the transition of electron from O $1s$ core level to the hybridized O $2p$- V t_{2g} and e_g states, which are crystal field splitted V $3d$ states. The crystal-field splitting ($10Dq$) of the LVO thin film is estimated to be ~1.3 eV from the energy separation between the t_{2g} and e_g structures. The magnitude of the $10Dq$ for the strained LVO thin film is smaller than that of the single crystal 1.8 eV [11]. To understand the rationale behind the decreased crystal field, we consider the ligand-field theory to qualitatively estimate the magnitude of $10Dq$, which is determined by the ion radius, electron mass, element number, and lattice constant [52]. The potential developed close to the center of the octahedron when point charge q is placed on each of the six corners of the octahedron is given by

$$\mathrm{V} \approx q/4\pi\varepsilon_o a[6 + 35/4a^4(x^4 + y^4 + z^4 + 3r^4/5) + \mathrm{O}(r^6/a^6)],$$

where x, y, z, and r are related to the Cartesian coordinates and "a" is the distance between the center of the octahedron and charge. It is clear from the above equation, if the metal to ligand distance is increased, the interaction potential is reduced and, as a result, the crystal field splitting energy is reduced. So, the enhancement of the out of plane lattice parameter in the strained LVO thin film led to the increase in V-O bond length and hence the $10Dq$ value is reduced. It is important to mention here that the hybridization strength ($pd\sigma$) between ligand $2p$ and metal $3d$ is determined from an overlap integral and mostly depends on the interatomic distances within the cluster [28]. Harrison proposed a relation of hybridization strength $(pd\sigma) \propto r_d^{1.5}/d_{\mathrm{M-O}}^{3.5}$, using the radial extent of the $3d$ orbital (r_d) and the metal-oxygen distance ($d_{\mathrm{M-O}}$) [53]. Therefore increase in the V-O bond length in the strained LVO film leads to the weaker hybridization between ligand and metal. The broad structure C, centered at 536 eV, in O K-edge spectrum is due to O $2p$ character mixed in the La $5d$ bands, which is, as expected, absent in the V_2O_3 or V_2O_5 spectrum. Higher energy features around 540–545 eV arise due to the O $2p$ and V $4s - 4p$ hybridized states, consistent with the reference V_2O_3 and the single-crystal $LaVO_3$ [45].

To further understand the V L-edge spectrum of strained LVO film, we have simulated the V^{3+} L-edge spectrum by using charge transfer multiplet program for x-ray absorption spectroscopy (CTM4XAS) [54] under the ligand field and charge transfer multiplet approach and compared it with the experimental spectrum. The shape of V L_3 and L_2 lines is very sensitive to the crystal field energy along with the vanadium ground state ($2p^6 3d^2$) as well as excited state ($2p^5 3d^3$) multiplet, which can be controlled by the two-particle interaction parameter. Therefore we performed charge transfer multiplet calculations by varying the reduction of Slater integrals, the crystal field splitting 10 Dq, charge transfer energy, d-d interaction energy, and O $2p$-V $3d$ hybridization strength. The simulated $L_{3,2}$ edge spectrum of V^{3+} with d^2 ($^3T_1$) ground state along with the experimental V L edge of strained $LaVO_3$ thin film is shown in Fig. 4(c). For simulation, the Slater integrals were reduced to 60% of the Hartree-Fock values and the crystal field in O_h symmetry was set at 1.3 eV. The values of other parameters used for the simulation are as follows: charge transfer energy (Δ) = 6.4 eV, $U_{2p3d} - U_{3d3d} = 2.2$ eV, and hopping parameter V (e_g) = 2.8 eV. The U_{3d3d} parameter defines the Hubbard U, which has no direct influence in case of a two-configuration charge transfer multiplet calculation for XAS; only the energy difference U_{2p3d}–U_{3d3d} is crucial, where the U_{2p3d} parameter defines the core-hole potential [54]. The hopping parameter (V) defines the hybridization between metal $3d$ orbitals and ligand $2p$ orbitals. V (e_g) and V (t_{2g}) are defined for the two different symmetries in O_h symmetry and are related to the $(x^2 - y^2,\ z^2)$ and $(xy,\ xz/yz)$ orbitals, respectively [54]. V (e_g) is related to the Slatter-Koster parameter ($pd\sigma$) by the relation V (e_g) $\approx \sqrt{3}(pd\sigma)$ [55]. The half-width of the Lorentzian and Gaussian line shapes is used in simulations to account for L_3 core-hole life time and instrumental broadening [48,51]. The Lorentzian of 0.3 eV and Gaussian of 0.25 eV are used for convolution of the simulated spectrum. Apart from these, several intrinsic broadening mechanisms eventuate along with the experimental broadening, and consequently, the experimental profile is more broadened as compared to the simulated profile [48]. Although the simulated and experimental profiles of V L edge agree well, the minor source of discrepancy could be due to the nonuniformity of the life time broadening. The simulated V^{3+} L-edge spectrum using the above parameter values [shown in Fig. 4(c)] is the best match with the experimental spectrum. Hopping parameters obtained from simulations suggest much weaker hybridization between V $3d$ and O $2p$ orbitals in the strained LVO film than the single crystal [28]. Here, it is important to mention that pre-edge features mostly arising due to a multiplet splitting are caused by the intra-atomic exchange and Coulomb interactions, which are represented by the Racah parameters or Slater integrals (F_2 and F_4) [1,48,51]. The reduction of two-particle interaction parameters (F_2 and F_4) is an alternative way to include the effect of hybridization effectively in the atomic multiplet calculations as suggested by the F. M. F. de Groot *et al.* [48]. As discussed above, the simulated spectrum with 60% reduction of the Slater integral in F_{dd} along with the $pd\sigma = 1.62$ eV yields the best match with the experimental spectrum. Therefore the less evident pre-peak

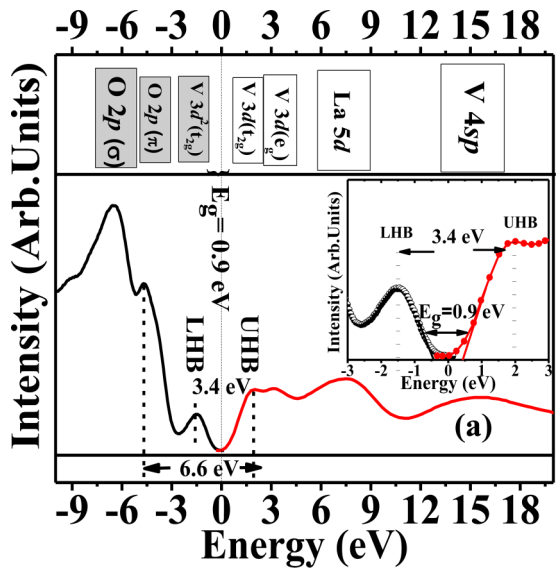

FIG. 5. (a) Combined valence and conduction bands along with a schematic band structure of the strained epitaxial $LaVO_3$ thin film. (Inset) Zoomed view of the band edge portion of combined spectra.

features below the V L edge are possibly due to the weaker hybridization between the V $3d$ and O $2p$ orbitals in strained LVO films.

3. *Electronic structure near the vicinity of the Fermi energy (E_F)*

In order to understand the band structure around the Fermi level in epitaxial strained $LaVO_3$ film, the experimental valance band and conduction band (oxygen K-edge) spectra are combined in a single frame of Fig. 5. For the valence band, we used the spectrum excitation on 56 eV with pass energy 15 eV due to its better resolution. The absence of spectral intensity at the Fermi level indicates the insulating nature of $LaVO_3$.

In the valence-band spectrum, the feature appearing at -1.5 eV below the E_F, assigned as an incoherent structure, has $3d$ character of vanadium. Even though previous reports [11,12] suggest a considerable O $2p$ character presence in this structure, the RPES studies of the $LaVO_3$ film confirm that the incoherent structure has a metal $3d$ character. Comparing the band-structure calculations [19,56], the observed incoherent feature is shifted by about 1 eV towards higher binding energy. Since the band-structure calculations within the local density approximation neglect the many-body interaction term, the shift towards higher binding energy reflects the strong electron correlation present in the strained epitaxial LVO film. The width (W) of this incoherent feature is about 2.1 eV. Therefore this localized incoherent structure represents the spectral signature of the lower Hubbard band (LHB) [13,19,57].

In order to analyze the conduction band (CB), we used the O K-edge spectrum because the states in the unoccupied band lie above the Fermi level and has the most weight on the metal site. In addition, the core-hole effect on the final state density of states (DOS) is less severe compared to the transitional metal $2p$ edge [58]. In the conduction band, three prominent features are observed at around 1.9, 3.2, and 7.5 eV and one broad feature is observed around 15 eV. The first two features are related to the unoccupied part of the t_{2g} and e_g bands, respectively, and the last one is attributed to the V $4s$-$4p$ band. It is important to mention that if the Coulomb repulsion energy U exceeds the bandwidth W, the Mott-Hubbard gap opens up between the lower Hubbard band (LHB) and upper Hubbard band (UHB) [1]. From the earlier reports [11,12,28], it is found that the reported value of U is much greater than the observed $3d$ bandwidth. Hence the spectroscopic signature of unoccupied t_{2g} states appearing at around 1.9 eV above E_F is attributed to the UHB [12,19,57]. Thus, from the combined spectra, U can be estimated as 3.4 eV and the charge transfer energy Δ: the energy difference between the O $2p$ band and UHB is observed to be 6.6 eV. These values are slightly towards the higher side than those observed for polycrystalline LVO ($U = 3$ eV and $\Delta = 6$ eV) [19]. Early TM compounds are expected to have strong hybridization between the ligand p and metal d orbitals for the larger spatial extent nature of $3d$ orbitals and, consequently, the weaker correlation effect. However, in our present study, we observed a smaller crystal field energy value compared to the single crystal suggesting the weaker ligand-p and metal-d hybridization in strained epitaxial LVO films. The enhanced out-of-plane lattice parameter due to the in plane compressive strain could be the reason for the weaker hybridization in strained epitaxial LVO systems as well as higher observed values of U and Δ than the previous estimation [19].

In order to estimate the gap between UHB and LHB, we draw a tangent at the point of inflection to find an approximate position of the band edges as shown in the inset of Fig. 5 and a band gap of about $\sim$0.9 eV is estimated. This value is slightly lower than the previous estimation by optical measurements, around 1.1 eV for polycrystalline LVO [59]. The physical properties of such Mott-Hubbard system is governed by U/W ratio, with $U/W > 1.15$ suggesting a Mott insulating state. The calculated value of the parameter $U/W \sim 1.61 > 1.15$, suggests a paramagnetic Mott insulating state of the system. The complete schematic band diagram is shown in Fig. 5. The observed findings are different from those reported for single-crystal LVO, which suggested that $U \sim \Delta$ and hence it was proposed that the LVO system should lie in the regime of charge transfer insulator and Mott-Hubbard insulator. However, in the present study, it is observed that the epitaxial $LaVO_3$ thin film shows the Mott-Hubbard insulating nature as $U < \Delta$.

(a) Effect of thickness. To examine the dimensionality effect on the on-site Coulomb interaction energy and the charge transfer energy of $LaVO_3$ thin films, we also recorded the VBS and XANES of thinner LVO films of thicknesses 2 and 8 nm, deposited under the same condition as used for 40 nm thick LVO film. The room-temperature VBS of the different thickness films recorded at a photon energy of 56 eV are shown in Fig. 6(a), which divulge that the line shape of V $3d$ band is slightly broadened in thinner films, more in the 2 nm than in the 8 nm LVO film, and is relatively shifted towards a lower binding energy value than in the 40 nm thick LVO film. The broadening of the V $3d$ band is attributed to the presence of an additional V^{4+} state, as also observed in its V core level spectra (not shown here). Wadati *et al.* [25] suggested that the origin of the V^{4+} state in such thinner films of LVO on LAO substrate was an outcome of electronic reconstruction at the interface of LVO and LAO and that the V^{4+} contribution decreased with increase in thickness. The

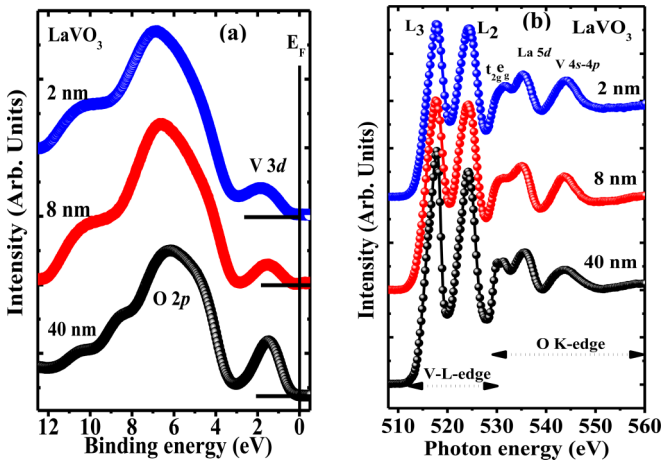

FIG. 6. (a) Room-temperature valence-band photoemission spectrum recorded at 56 eV photon energy with 20 eV pass energy of the 2 nm, 8 nm and 40 nm $LaVO_3$ thin films and (b) room-temperature XANES of the 2 nm, 8 nm and 40 nm $LaVO_3$ thin films.

minor shift in V 3*d* band position towards a lower binding energy position has also been attributed by Wadati *et al.* to the increase in U as a consequence of decrease in dielectric screening in thinner samples [25]. The O 2*p* position in the VBS remains same for all the films. The V $L_{3,2}$ and O K-edge absorption spectra of all the films, shown in Fig. 6(b), exhibits somewhat similar behavior with the photon energy, albeit, the two features at 530.1 and 531.4 eV observed in the O K edge of 40 nm thick film representing the t_{2g} and e_g bands are merged and form a broad structure with a minor shift in position towards a higher photon energy value in thinner LVO films. The intensity ratio of L_3 to L_2 absorption peaks decreases slightly in the 2 nm and 8 nm LVO films compared to the 40 nm thick LVO film, due to the additional contribution of the V^{4+} state [48].

The combined electronic structure near E_F is shown in Fig. 7(a). It is clear that the binding energy position of the V 3*d* band is shifted to a lower energy position in the 2 nm thin LVO films compared to the 8 nm or 40 nm thick LVO films. From the combined occupied and unoccupied states considering the LHB and UHB positions, the value of U for the 2 nm thin LVO film is estimated as 4.1 eV, whereas for the 8-nm LVO film, U deceases to 3.7 eV. The charge transfer gap Δ: the energy difference between the O 2*p* band and UHB, also increases with decrease in thickness (~6.6 eV for 40 nm film and 6.9 eV for 2 nm LVO film). The values of Δ in all the films are higher than the U values of the respective films, suggesting that the LVO films of lower thicknesses also divulge the Mott-Hubbard insulating nature.

IV. DISCUSSIONS

The early TM compounds, mainly the Ti and V oxides have been considered as a Mott-Hubbard system [60]. Based on the cluster model analysis, earlier studies [11,12,28] suggested that bulk $LaVO_3$ along with few early transition metal oxide compounds should be placed intermediate between the charge transfer and Mott-Hubbard regime owing to the equivalent values of U and Δ (~4 eV). In these studies, the early TM compounds were characterized by a large *p-d* hybridization,

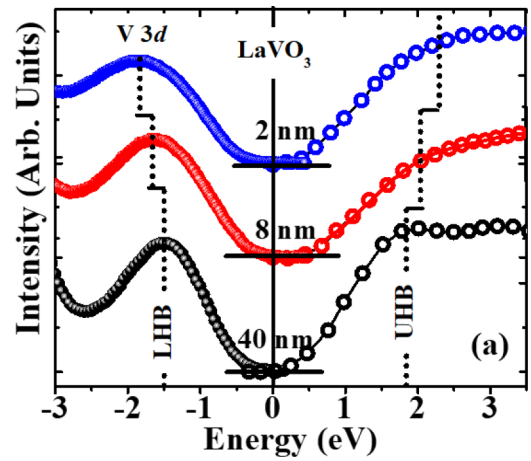

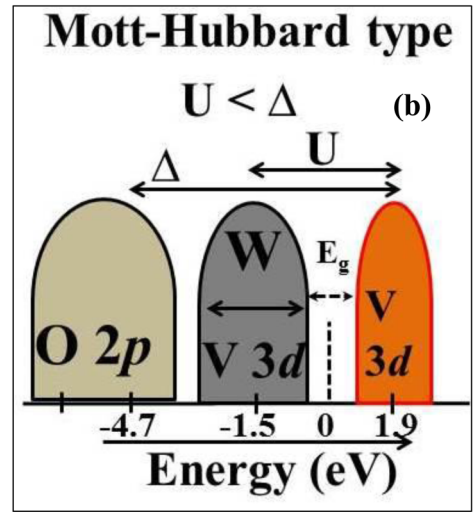

FIG. 7. (a) Combined valence and conduction bands of the 2 nm, 8 nm and 40 nm $LaVO_3$ thin films near Fermi level. (b) Schematic illustration of the Mott-Hubbard type insulating nature of the epitaxial $LaVO_3$ thin film.

which led to the strong covalency in those compounds. As a result, a considerable amount of O 2*p* character ($3d^n\underline{L}$) was present in the incoherent feature (near E_F) of $LaVO_3$ and consequently it could not be assigned as an LHB and the charge transfer energy was reduced [12].

It is quite interesting to highlight that the strong screening of the 3*d* hole by the charge transfer from anion atoms ($3d^n\underline{L}$) has been found in the photoemission spectra mostly of the heavy 3*d* transitional metal oxides. It has been suggested that such screening effect by charge transfer is small for light transition-metal oxide compounds [61]. It is worthwhile to mention that the CIS spectra of the $3d^n\underline{L}$ final state gives an anti-resonance dip that is mostly evident for the heavy transition-metal compounds, whereas those of the $3d^{n-1}$ final state exhibits a simple resonance enhancement without a remarkable antiresonance deep. Interestingly such antiresonance dip in the CIS spectra of V 3*d* feature was absent in CIS plot of feature A, pointing out towards the $3d^{n-1}$ like final state, ascribed to the incoherent structure. It is essential to mention that 3*d* orbitals of late TM are localized in nature. However,

despite its localized nature of the 3*d* orbitals, the e_g orbitals of the heavy TM oxide system can strongly hybridize with the oxygen *p* orbitals to form the e_g bands with appreciable bandwidth. Studies on manganite based thin films give clear understanding of strain effect on e_g bands in terms of lattice effects on the *p*-*d* hybridization [62,63]. On the other hand the t_{2g} band of $LaVO_3$ is quite narrow due to the weak *p*-*d* hybridization, which will account for the $3d^{n-1}$ final state of the incoherent feature. The dynamical mean-field theory (DMFT) also attributes this incoherent structure to the $3d^{n-1}$ final state configuration [57]. Therefore the V 3*d* character of the incoherent band is attributed to the lower Hubbard band. Hence the spectroscopic investigation suggests the Mott-Hubbard insulating nature of epitaxial $LaVO_3$ film whose physical properties are primarily governed by the strength of U/W. The simulated spectrum [Fig. 4(c)] also reflects a good agreement with the different physical parameters as we obtained from the combined LHB+UHB spectra and is concomitant with the Mott Hubbard insulating nature of epitaxial $LaVO_3$ thin films. A schematic illustration of the Mott-Hubbard type insulating nature of strained epitaxial LVO thin film is shown in Fig. 7(b).

Earlier reports suggested that the LVO should be placed intermediate between Mott-Hubbard and charge transfer. However, the current study confirms the weaker hybridization between V 3*d* and O 2*p* states in strained epitaxial LVO thin films and suggests its Mott-Hubbard insulating character. It has also been claimed that the substrate induced strain modifies the V-O-V bond angle of LVO with respect to its bulk orthorhombic structure, and hence substrate induced stress has an immense role in the orbital overlapping in thin films resulting in a lower charge transfer splitting, decrease in hybridization strength, and lowering of the Mott gap [64]. So it is possible to tune the metal-ligand hybridization with the help of substrate induced stress. Therefore, by using the substrate induced stress along with two-dimensional effects; one can modify the band structure of LVO film through the control over W, U, and Δ. Such modifications may have profound effects on the physical properties of 2D heterostructures involving LVO. It is important to mention here that two-dimensionality usually enhances the electron correlation effect as has been observed in the present study also with enhanced U values in the 2 nm thin LVO film than the 40 nm thin LVO film.

V. CONCLUSIONS

We have probed the electronic properties of the epitaxial thin films of (001) oriented $LaVO_3$ grown on $LaAlO_3$ substrate by pulsed laser deposition. The film, due to in-plane compressive strain, shows enhancement of the out of plane lattice parameter. Cube-on-cube epitaxial growth of LVO on LAO substrate is confirmed by the in-plane Φ scan. The smaller crystal field energy value calculated from O *K*-edge XANES and the hopping parameter obtained from the simulation of V *L* edge suggest a weaker ligand-*p* and metal-*d* hybridization in strained LVO film. The photon energy dependence of the valence-band spectra confirms the V 3*d* character of the incoherent structure near the E_F. The resonance enhancement at 6.9 eV in the O 2*p* band confirms the mixing of V 3*d* with O 2*p* present in the O 2*p* derived state of the valence band. Our present work based on RPES and XANES measurements confirms that the V 3*d* character with $3d^{n-1}$ final state is responsible for the incoherent band and is attributed as a lower Hubbard band. Combination of photoemission and absorption spectra suggests the Mott-Hubbard type insulating state of $LaVO_3$ thin films at room temperature. The weaker hybridization between O 2*p* and V 3*d* in the present LVO films leads to a higher charge transfer energy compared to bulk LVO.

ACKNOWLEDGMENTS

The authors would like to thank F. M. F. de Groot for important discussions regarding the x-ray absorption spectra. Authors are also thankful to V. R. Reddy for phi scan measurement. Authors also acknowledge A. Wadikar, Sharad Karwal, and Rakesh Sah for help during RPES and XANES measurements.

[1] M. Imada, A. Fujimori, and Y. Tokura, Rev. Mod. Phys. **70**, 1039 (1998).
[2] C. N. R. Rao and B. Raveau, *Transition Metal Oxides*, 2nd ed. (Wiley, New York).
[3] M. Takizawa, Y. Hotta, T. Susaki, Y. Ishida, H. Wadati, Y. Takata, K. Horiba, M. Matsunami, S. Shin, M. Yabashi, K. Tamasaku, Y. Nishino, T. Ishikawa, A. Fujimori, and H. Y. Hwang, Phys. Rev. Lett. **102**, 236401 (2009).
[4] F. Inaba, T. Arima, T. Ishikawa, T. Katsufuji, and Y. Tokura, Phys. Rev. B **52**, R2221(R) (1995).
[5] H. C. Nguyen and J. B. Goodenough, Phys. Rev. B **52**, 324 (1995).
[6] A. V. Mahajan, D. C. Johnston, D. R. Torgeson, and F. Borsa, Phys. Rev. B **46**, 10966 (1992).
[7] P. Bordet, C. Chaillout, M. Marezio, Q. Huang, A. Santoro, S. W. Cheong, H. Takagi, C. S. Oglesby, and B. Batlogg, J. Solid State Com. **106**, 253 (1993).
[8] S. Miyasaka, Y. Okimoto, M. Iwama, and Y. Tokura, Phys. Rev. B **68**, 100406(R) (2003).
[9] N. Shirakawa and M. Ishikawa, Jpn. J. Appl. Phys. **30**, L755 (1991).
[10] S. Yoon, J. Appl. Phys. **105**, 07D509 (2009).
[11] R. J. O. Mossanek, M. Abbate, T. Yoshida, A. Fujimori, Y. Yoshida, N. Shirakawa, H. Eisaki, S. Kohno, and F. C. Vicentin, Phys. Rev. B **78**, 075103 (2008).
[12] R. J. O. Mossanek, M. Abbate, T. Yoshida, A. Fujimori, Y. Yoshida, N. Shirakawa, H. Eisaki, H. Eisaki, S. Kohono, P. T. Fonseca, and F. C. Vicentin, J. Phys.: Condens. Matter, **22**, 095601 (2010).
[13] A. Fujimori, I. Hase, H. Namatame, Y. Fujishima, Y. Tokura, H. Eisaki, S. Uchida, K. Takegahara, and F. M. F. de Groot, Phys. Rev. Lett. **69**, 1796 (1992).
[14] K. Morikawa, T. Mizokawa, K. Kobayashi, A. Fujimori, H. Eisaki, S. Uchida, F. Iga, and Y. Nishihara, Phys. Rev. B **52**, 13711 (1995).

[15] M. J. Rozenberg, I. H. Inoue, H. Makino, F. Iga, and Y. Nishihara, Phys. Rev. Lett. **76**, 4781 (1996).

[16] E. Pavarini, S. Biermann, A. Poteryaev, A. I. Lichtenstein, A. Georges, and O. K. Andersen, Phys. Rev. Lett. **92**, 176403 (2004).

[17] J. B. Webb and M. Sayer, J. Phys. C: Solid State Phys. **9**, 4151 (1976).

[18] A. V. Mahajan, D. C. Johnston, D. R. Torgeson, and F. Borsa, Phys. Rev. B **46**, 10973 (1992).

[19] K. Maiti and D. D. Sarma, Phys. Rev. B **61**, 2525 (2000).

[20] M. Kasuya, Y. Tokura, T. Arima, H. Eisaki, and S. Uchida, Phys. Rev. B **47**, 6197 (1993).

[21] E. Janod, J. Tranchant, B. Corraze, M. Querré, P. Stoliar, M. Rozenberg, T. Cren, D. Roditchev, V. T. Phuoc, M.-P. Besland, and L. Cario, Adv. Funct. Mater. **25**, 6287 (2015).

[22] L. Wang, Y. Li, A. Bera, C. Ma, F. Jin, K. Yuan, W. Yin, A. David, W. Chen, W. Wu, W. Prellier, S. Wei, and T. Wu, Phys. Rev. Appl. **3**, 064015 (2015).

[23] H.-T. Zhang, M. Brahlek, X. Ji, S. Lei, J. Lapano, J. W. Freeland, V. Gopalan, and R. E. Herbert, ACS Appl. Mater. Interf. **9**, 12556 (2017).

[24] Y. Hotta, T. Susaki, and H. Y. Hwang, Phys. Rev. Lett. **99**, 236805 (2007).

[25] H. Wadati, Y. Hotta, A. Fujimori, T. Susaki, H. Y. Hwang, Y. Takata, K. Horiba, M. Matsunami, S. Shin, M. Yabashi, K. Tamasaku, Y. Nishino, and T. Ishikawa, Phys. Rev. B **77**, 045122 (2008).

[26] H. Wadati, Y. Hotta, M. Takizawa, A. Fujimori, T. Susaki, and H. Y. Hwang, J. Appl. Phys. **102**, 053707 (2007).

[27] Y. Hotta, H. Wadati, A. Fujimori, T. Susaki, and H. Y. Hwang, Appl. Phys. Lett. **89**, 251916 (2006).

[28] A. E. Bocquet, T. Mizokawa, K. Morikawa, A. Fujimori, S. R. Barman, K. Maiti, D. D. Sharma, Y. Tokura, and M. Onoda, Phys. Rev. B **53**, 1161 (1996).

[29] S. J. Gharetape, M. P. Sing, F. S. Razavi, D. A. Crandles, L. Y. Zhao, and K. T. Leung, Appl. Phys. Lett. **98**, 052509 (2011).

[30] R. P. Gupta and S. K. Sen, Phys. Rev. B **12**, 15 (1975).

[31] F. M. F. de Groot, Coord. Chem. Rev. **249**, 31 (2005).

[32] M. C. Biesinger, L. W. M. Lau, A. R. Gerson, and R. St. C. Smart, Appl. Surf. Sci. **257**, 887 (2010).

[33] C. D. Wagner, W. M. Riggs, L. E. Davis, and J. F. Moulder, *Handbook of X-ray Photoelectron Spectroscopy* (Perkin-Elmer Corporation, 1978).

[34] R. Bindu, G. Adhikary, N. Sahadev, N. P. Lalla, and K. Maiti, Phys. Rev. B **84**, 052407 (2011).

[35] R. G. Egdell, M. R. Harrison, M. D. Hill, L. Porte, and G. Wall, J. Phys. C: Solid State Phys. **17**, 2889 (1984).

[36] K. E. Smith and V. E. Henrich, Phys. Rev. B **38**, 5965 (1988).

[37] J. J. Yeh and I. Lindau, At. Data Nucl. Data Tables **32**, 1 (1985).

[38] L. C. Davis, J. Appl. Phys. **59**, R25 (1986).

[39] K. E. Smith and V. E. Henrich, Phys. Rev. B **38**, 9571 (1988).

[40] J. Barth, F. Gerken, and C. Kunz, Phys. Rev. B **31**, 2022 (1985).

[41] J. Barth, F. Gerken, K. L. I. Kobayashi, J. H. Weaver, and B. Sonntag, J. Phys. C **13**, 1369 (1980).

[42] E. Bertel, R. Stockbauer, and T. E. Madey, Phys. Rev. B **27**, 1939 (1983).

[43] S. Shin, S. Suga, M. Taniguchi, M. Fujisawa, H. Kanzaki, A. Fujimori, H. Daimon, Y. Ueda, K. Kosuge, and S. Kachi, Phys. Rev. B **41**, 4993 (1990).

[44] H. F. Pen, M. Abbate, A. Fujimori, Y. Tokura, H. Eisaki, S. Uchida, and G. A. Sawatzky, Phys. Rev. B **59**, 7422 (1999).

[45] B. Chen, J. Laverock, D. Newby Jr, J. F. McNulty, K. E. Smith, P.-A. Glans, F.-H. Guo, R.-M. Qiao, W.-L. Yang, M. R. Lees, L. D. Tung, R. P. Singh, and G. Balakrishnan, J. Phys.: Condens. Matter **27**, 105503 (2015).

[46] J. Laverock, B. Chen, A. R. H. Preston, D. Newby, L. F. J. Piper, L. D. Tung, G. Balakrishnan, P.-A. Glans, J.-H. Guo, and K. E. Smith, J. Phys.: Condens. Matter **26**, 455603 (2014).

[47] J. Laverock, B. Chen, A. R. H. Preston, K. E. Smith, N. R. Wilson, G. Balakrishnan, P.-A. Glans, and J.-H. Guo, Phys. Rev. B **87**, 125133 (2013).

[48] F. M. F. de Groot, J. C. Fuggle, B. T. Thole, and G. A. Sawatzky, Phys. Rev. B **42**, 5459 (1990).

[49] J. Zaanen, G. A. Sawatzky, J. Fink, W. Speier, and J. C. Fuggle, Phys. Rev. B **32**, 4905 (1985).

[50] D. Ruzmetov, S. D. Senanayake, and S. Ramanathan, Phys. Rev. B **75**, 195102 (2007).

[51] G. Van der Laan and I. W. Kirkman, J. Phys.: Condens. Matter **4**, 4189 (1992).

[52] Y. Shimazu, T. Okumura, A. Shimada, K. Tanabe, K. Tokiwa, E. Sakai, H. Kumigashira, and T. Higuchi, Jpn. J. Appl. Phys. **53**, 06JG05 (2014).

[53] W. A. Harrison, *Electronic Structure and Physical Properties of Solids* (Freeman, San Francisco, 1980).

[54] E. Stavitski and F. M. F. de Groot, Micron **41**, 687 (2010).

[55] A. E. Bocquet, T. Mizokawa, T. Saitoh, H. Namatame, and A. Fujimori, Phys. Rev. B **46**, 3771 (1992).

[56] V. I. Anisimov, J. Zaanen, and O. K. Andersen, Phys. Rev. B **44**, 943 (1991).

[57] I. A. Nekrasov, G. Keller, D. E. Kondakov, A. V. Kozhevnikov, Th. Pruschke, K. Held, D. Vollhardt, and V. I. Anisimov, Phys. Rev. B **72**, 155106 (2005).

[58] F. M. F. de Groot, M. Grioni, J. C. Fuggle, J. Ghijsen, G. A. Sawatzky, and H. Petersen, Phys. Rev. B **40**, 5715 (1989).

[59] T. Arima, Y. Tokura, and J. B. Torrance, Phys. Rev. B **48**, 17006 (1993).

[60] J. Zaanen, G. A. Sawatzky, and J. W. Allen, Phys. Rev. Lett. **55**, 418 (1985).

[61] G. A. Sawatzky and J. W. Allen, Phys. Rev. Lett. **53**, 2339 (1984).

[62] B. R. K. Nanda and S. Satpathy, Phys. Rev. B **78**, 054427 (2008).

[63] P.-H. Xiang, H. Yamada, A. Sawa, and H. Akoh, Appl. Phys. Lett. **94**, 062109 (2009).

[64] H. Rotella, U. Luders, P.-E. Janolin, V. H. Dao, D. Chateigner, R. Feyerherm, E. Dudzik, and W. Prellier, Phys. Rev. B **85**, 184101 (2012).